Modal study of the role of excess noise in x-ray lasers

Peter Amendt and Richard A. London
Lawrence Livermore National Laboratory, University of California, P.O. Box 808, Livermore, California 94550

Moshe Strauss
Physics Department, Nuclear Research Centre-Negev, Beer Sheva 84190, Israel
(Received 15 October 1990; revised manuscript received 22 February 1991)

Current x-ray laser designs rely on amplifying spontaneous emission in a high-temperature plasma. A central problem in the study of x-ray lasers is determining and optimizing the degree of transverse spatial coherence for holographic applications. The inherent non-power-orthogonal character of the normal modes in a general amplifying medium necessarily results in excess noise and cross-correlation effects that can significantly affect the predicted coherence and intensity profiles of an x-ray laser. In particular, loosely bound discrete transverse eigenstates of the paraxial wave equation have previously been found to dominate the intensity and coherence in the low-amplification regime if the continuum eigenstates are omitted from the spectrum [London, Strauss, and Rosen, Phys. Rev. Lett. **65**, 563 (1990)]. A detailed analysis of the role of excess noise on steady-state laser intensity and coherence is presented for the simple case of a transverse square gain and density profile in a finite geometry. The inclusion of the continuum portion of the spectrum is found to substantially reduce the level of excess noise and to alter the coherence predictions for low and intermediate gain-length products.

PACS number(s): 42.50.Ar, 42.55.Vc, 42.60.Da, 52.25.Nr

I. INTRODUCTION

The recent demonstration of x-ray lasing near the carbon K edge (≈ 43.7 Å) in Ni-like tantalum and tungsten brings closer the feasibility of holographic imaging of wet biological samples [1,2]. A key requirement in holographic applications of x-ray lasers is adequate coherence, both in the longitudinal (temporal) and transverse (spatial) directions. The longitudinal coherence appears sufficient based on measured and estimated intrinsic linewidths. For example, in Ni-like Ta the width $\Delta\lambda$ of the 44.8-Å line is estimated to be less than the intrinsic Doppler line profile width of 5 mÅ, giving a longitudinal coherence length of $\lambda^2/\Delta\lambda$ greater than 37 μm. Recent measurements of the 206-Å Ne-like Se line profile in fact support this argument [3]. Because this coherence length far exceeds the path-length difference between the object and reference beam in current x-ray laser holography designs [4], longitudinal coherence appears to be satisfactory. The situation is more problematic for transverse coherence where the required coherence length (at the position of the object) must exceed the transverse dimension of the object, which is typically about 10 μm, and the photon fluence must exceed some minimum value [2]. In practice, these conditions generally mean that we must require a coherence length at least comparable to the lasing half-width, giving a significant fraction ($>10\%$) of the output energy as coherent energy. As London, Rosen, and Strauss have recently suggested [5], the most direct way of improving the transverse coherence is to increase the gain-length product in concert with gain-guiding and refractive-defocusing effects. Unfortunately, the use of cavities to increase the effective gain-length product is hindered by current x-ray mirror technology (particularly at shorter wavelengths) and by the short lifetime (~ 100 psec) of the lasing plasma equilibrium state. At present, one particularly promising approach towards improved transverse coherence relies on the use of multistage (oscillator-amplifier) architectures with spatial filtering [6].

There are at present two main analytic approaches to understanding x-ray laser coherence: (1) expanding the electric field in terms of a longitudinally coupled orthogonal basis set and then solving for the electric-field correlation function by Green's-function techniques [7,8], or (2) employing a longitudinally decoupled nonorthogonal (and possibly incomplete) set and solving directly for the correlation function [5,9,10]. The former procedure has the advantage of avoiding altogether the completeness problem for the spectral basis, but suffers from a difficult implementation. The second technique, or modal approach, involves solving a Schrödinger-type equation with a complex potential where the associated eigenfunctions possibly may not constitute a complete set. The main advantage of the modal approach lies in the relative simplicity of solving for the mode spectrum, which, we argue, more closely agrees with the conventional description of the normal modes of a lasing medium, e.g., in terms of Fox-Li transverse resonator modes.

The modal method has recently been used to understand some basic properties of x-ray laser coherence for a few simple transverse gain and density profiles [2]. The square gain profile permits a considerable degree of analytic progress and thus has served as a useful model to describe some of the essential aspects of x-ray laser coherence. The spectrum associated with the transverse square profile consists partially of a set of discrete bound states or "laser" modes that dominates the intensity for

sufficiently large gain-length product. These modes were exclusively considered by London, Rosen, and Strauss in their study of x-ray laser coherence [5]. A key finding in their analysis is that the total intensity and coherence profiles are particularly sensitive to the gain strength. Specifically, if the gain is increased by an infinitesimal amount, a very marginally bound mode may suddenly emerge that can dominate the intensity at large transverse distances away from the lasing medium (see Fig. 1). This phenomenon is not at all new; it is related to excess spontaneous noise that arises from the inherently non-self-adjoint character of any amplifying medium [10,11]. A conventional measure of excess spontaneous emission is the so-called Petermann factor, which equals unity in the absence of gain and can be much larger than one if the mode is loosely bound or marginally localized [12]. An understanding of excess spontaneous noise is of paramount importance in determining and optimizing transverse coherence in current x-ray-laser experiments.

In this paper we emphasize that the continuum portion of the spectrum must be considered in addition to the bound modes for a proper description of x-ray laser intensity and coherence, as originally suggested by London, Rosen, and Strauss [5]. Our contribution in this work is to study in detail how the properties of excess spontaneous noise are affected when unbound or continuum normal modes are included in the spectrum. It is found that the aforementioned sensitivity of the electric-field intensity on the gain strength largely disappears when bound and unbound modes are treated together. As a consequence, the contribution to the electric-field intensity outside of the lasing medium from loosely bound modes is greatly reduced, thereby effectively lowering the value of the Petermann factor. The explanation for such a reduced level of excess spontaneous noise is that the normal modes are often highly cross-correlated and provide the required cancellation when a presumably complete spectrum is considered. This behavior is not limited to very short amplifiers where no gain discrimination occurs [9], but also arises in systems with moderately large gain-length product. In brief, the inclusion of the continuum affects the overall intensity and coherence profiles for gain-length products that are presently of experimental relevance by mostly eliminating what is often characterized as excess noise.

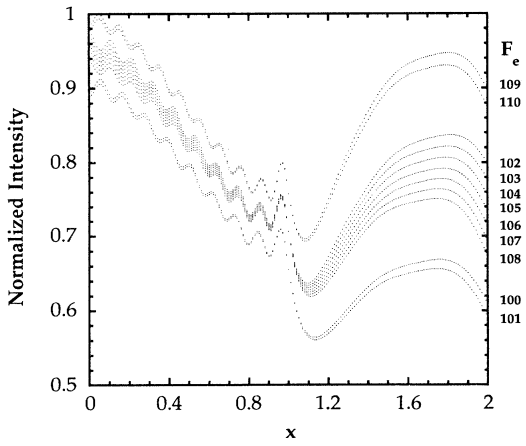

FIG. 1. Shown are intensity profiles using only bound modes as in London, Rosen, and Strauss [5] as a function of normalized transverse position x when the strength of the gain as measured by F_e is slightly varied from 100 to 110. Note the particular sensitivity of the intensity profiles beyond $x=1$ as F_e is raised and new bound modes are created.

We organize the paper as follows. In Sec. II we consider square transverse gain and density profiles in a finite geometry and analyze the full spectrum of eigenmodes. We then proceed to show, both analytically and with numerical examples, how the inclusion of the continuum provides the required cancellation of global intensity due to one loosely bound mode. In Sec. III we study in detail local intensity and coherence profiles and explore how they each differ in the absence of the continuum modes. We present a summary and conclude in Sec. IV.

II. ANALYSIS

A. Mode equations

Our starting point for investigating the role of excess noise in x-ray laser optics is the scalar wave equation for the transverse component of the electric-field E

$$\nabla^2 E-\frac{1}{c^2}\frac{\partial^2 E}{\partial t^2}=\frac{4\pi}{c^2}\left[\frac{\partial P}{\partial t}+J\right], \tag{1}$$

where P is the atomic polarization responsible for spontaneous and stimulated emission (or absorption), and J is the current density. We assume that the current density is due only to the free electrons of the plasma, giving $\partial J/\partial t=(\omega_p^2/4\pi)E$, where $\omega_p\approx 5.64\times 10^4\, n_e^{1/2}\,\mathrm{rad\,s^{-1}}$ is the electron plasma frequency and n_e is the electron density. We next make a slowly varying envelope approximation for the electric field and atomic polarization as follows:

$$E(\mathbf{r},t)=\mathcal{E}_\omega(\mathbf{r})e^{i(\omega t-kz)}+\text{c.c.}\ ,$$

$$P(\mathbf{r},t)=\mathcal{P}_\omega(\mathbf{r})e^{i(\omega t-kz)}+\text{c.c.}\ ,$$

where $k=\omega/c$ is the free space wave number and the ω subscript on the fields refers to one Fourier component of the electric field traveling in the positive z direction. In steady state we may write $P_\omega=iK_\omega E_\omega+P_{\mathrm{sp}}$, where the first expression describes stimulated processes and the second term represents a random polarization source that is associated with spontaneous emission [13]. The response function $K_\omega(\mathbf{r})=(\pi d_{21}^2/3\hbar)N(\mathbf{r})\psi(\omega)$ is proportional to the gain, where d_{21} is the dipole matrix element for the $n=2\rightarrow n=1$ atomic transition, $\Delta N(\mathbf{r})$ is the atomic population inversion per unit volume, and $\psi(\omega)$ is the line profile function (or imaginary part of the atomic susceptibility) normalized by the condition $\int\psi(\omega)d\omega=1$. We assume that the transition is unsaturated, so that ΔN is independent of E_ω.

The particular physical system we wish to study is that of a plasma uniform in the z direction that can support amplified spontaneous emission (ASE), given a set of

transverse profiles for the gain and electron density. For typical ASE x-ray laser experiments prepared by intense line focusing [1], we may further assume that the system is homogeneous in the y direction as also commonly adopted in stripe geometry solid-state laser modeling [14]; the extension to a two-dimensional (2D) transverse system is straightforward but will not be considered here.

A steady-state paraxial wave equation follows from Eq. (1) by substituting the above definitions and assuming $|\partial^2 E_\omega/\partial z^2| \ll |2k\partial E_\omega/\partial z|$ or $|\partial^2 E_\omega/\partial x^2|$ [15]:

$$\left[\frac{1}{k}\nabla_\perp^2 - 2i\frac{\partial}{\partial z} - h(x) + ig(x,\omega)\right]E(\mathbf{r}) = -4\pi k P_{\rm sp}(\mathbf{r}) , \tag{2}$$

where $\nabla_\perp^2$ is the transverse Laplacian, $h(x)=\omega_p^2(x)/kc^2$ is the refraction strength, and $g(x,\omega)=4\pi^2 d_{21}^2 k\psi(\omega)\Delta N/3\hbar$ is the frequency-dependent gain coefficient. In the modal approach, a solution to Eq. (2) is sought by writing the electric-field amplitude E_ω as a (presumably complete) mode expansion of longitudinal and transverse factors:

$$E_\omega(\mathbf{r}) = \sum_n c_n(z)u_n(x) , \tag{3}$$

where the transverse functions or modes $u_n(x)$ are eigenfunctions of the paraxial equation *without* the spontaneous-emission source term:

$$\left[\frac{\partial^2}{\partial x^2} - F_e[\eta\hat{h}(x) - i\hat{g}(x)]\right]u_n(x) = -E_n u_n(x) , \tag{4}$$

and the longitudinal functions $c_n(z)$ satisfy

$$\sum_n \left[u_n\frac{\partial c_n}{\partial z} - \frac{i}{2}E_n c_n u_n\right] = -iP_{\rm sp} . \tag{5}$$

In Eqs. (4) and (5), E_n labels the eigenvalue ($E_n=-2ika^2q_n$ of London, Rosen, and Strauss [5]) and we have rescaled all quantities according to the following prescription: $x\to xa$, $z\to zka^2$, $P_{\rm sp}\to P_{\rm sp}/2\pi(ka)^2$, $h\to h/h_0\equiv\hat{h}$, $g\to g/g_0\equiv\hat{g}$, where h_0 denotes a mean refraction strength, g_0 is an average value of gain, and a is a representative width of the lasing medium. We also have introduced the dimensionless parameters F_e and η, where $F_e=kg_0a^2$ is an effective Fresnel number for an amplifying medium, and $\eta=h_0/g_0$ provides a measure of the relative strengths of refraction and gain.

Equation (4) is a Schrödinger-type equation with a complex potential. Because of the non-self-adjoint properties of such an equation, the eigenvalues E_n are generally complex, the eigenfunctions $u_n(x)$ are not mutually orthogonal, and the spectrum of eigenfunctions may not be complete in general [16]. The first two properties are of clear physical relevance to ASE systems, but the last one presents a mathematical complication about which we can say very little in general. A proof of completeness exists for the special case of unbounded parabolic gain and refraction profiles, but the physical appropriateness of such an example is not clear. For most ASE x-ray laser experiments the refraction strength parameter η is much larger than unity, and the gain contribution to the "potential" in Eq. (4) may be viewed as a small perturbation to the zero-order continuum portion of the spectrum, which is complete for a finite "potential." However, the discrete modes are not describable by conventional perturbation techniques, and although they represent only a "small" yet finite contribution to the full spectrum, their inclusion is essential for all values of the gain-length product. For the square gain profile that we will consider shortly, a qualitative measure of completeness will be presented that allows us to gauge the degree to which our adopted spectrum is complete.

It is straightforward to show that the eigenfunctions of Eq. (4) are *biorthonormal* in the following sense: $\int u_n u_m dx = \delta_{nm}$, and satisfy the following identity:

$$(E_n - E_m^*)\int_{-A}^{A} u_n u_m^* dx + 2iF_e\int_{-A}^{A}\hat{g}u_n u_m^* dx = 0 , \tag{6}$$

provided the operator ∂_{xx}^2 is Hermitian with respect to the eigenfunctions u_n and u_m, which satisfy the boundary condition $u_n^* du_m/dx|_{x=-A} = u_n^* du_m/dx|_{x=A}$. We will shortly construct eigenfunctions for the square profile that satisfy homogeneous boundary conditions at the boundaries $x=\pm A$ and thereby permit use of Eq. (6). Using the biorthonormal property of the eigenfunctions and a chosen normalization $\int u_n^2 dx = 1$, we find the following equation for the longitudinal functions $c_n(z)$:

$$\frac{dc_n(z)}{dz} = \frac{i}{2}E_n c_n - ip_n , \tag{7}$$

where p_n is the projection of the spontaneous polarization term onto the nth eigenfunction:

$$p_n = \int u_n P_{\rm sp} dx . \tag{8}$$

The quantity of main interest is the two-point electric-field correlation function in space $\langle E_\omega(\mathbf{r}_1)E_\omega^*(\mathbf{r}_2)\rangle$, where the angular brackets indicate an ensemble average. This is conventionally called the mutual intensity in the optics literature [17]. For $\mathbf{r}_1=\mathbf{r}_2$, the correlation function reduces to the radiation energy density, while for $\mathbf{r}_1\neq\mathbf{r}_2$, it describes the degree of spatial coherence of the field. From the mode expansion given by Eq. (3), we can write for the correlation function:

$$\langle E_\omega(\mathbf{r}_1)E_\omega^*(\mathbf{r}_2)\rangle = \sum_{n,m}\langle c_n(z_1)c_m^*(z_2)\rangle u_n(x_1)u_m^*(x_2) . \tag{9}$$

The correlation term $\langle c_n c_m^*\rangle$ is found by formally solving Eq. (7) for $c_n(z)$ and then taking the ensemble average of the product, which will involve a term of the form $\langle p_n p_m^*\rangle$. This spontaneous emission is assumed to be δ-function correlated in space, since all length scales of interest are much larger than the interatomic spacing, and the spontaneous emission from different atoms is expected to be uncorrelated. The normalization is determined by equating the classical radiation from an ensemble-averaged dipole moment per unit volume to the atomic spontaneous radiation given by the Einstein relations [10], yielding

$$\langle P_{\rm sp}(\mathbf{r}_1)P^*_{\rm sp}(\mathbf{r}_2)\rangle = 8\pi^2 F_e \hat{g}(x,\omega)\hbar\Delta\omega\frac{N_2}{\Delta N}(k/a^2) \times\delta(\mathbf{r}_1-\mathbf{r}_2)\ , \tag{10}$$

where N_2 is the upper atomic state number density and $\Delta\omega$ is the full width at half maximum (FWHM) linewidth of the atomic transition. From Eqs. (6) (7), and (10) we easily find

$$\langle c_n(z)c^*_m(z)\rangle = C_1(e^{iz(E_n-E^*_m)/2}-1)B_{nm}\ , \tag{11}$$

where $C_1=8\pi^2\hbar\Delta\omega(k/a^2)N_2/\Delta N$ is assumed to be constant, and $B_{nm}=\int u_n u^*_m dx (\neq\delta_{nm})$. In Eq. (11) we have taken $\langle c_n(0)c^*_m(0)\rangle=0$, so that only the amplification of modal emission from within the lasing medium ($0\le z\le L$) is considered.

We define the coherence function as the absolute value of the complex coherence factor [18]:

$$\mu(x_1,x_2;z)=\left|\frac{\langle E_\omega(x_1,z)E^*_\omega(x_2,z)\rangle}{[\langle E_\omega(x_1,z)E^*_\omega(x_1,z)\rangle]^{1/2}[\langle E_\omega(x_2,z)E^*_\omega(x_2,z)\rangle]^{1/2}}\right| . \tag{12}$$

For example, μ is the fringe visibility in a two-slit interferometer when $\langle E_\omega(x_1,z)E^*_\omega(x_1,z)\rangle = \langle E_\omega(x_2,z)E^*_\omega(x_2,z)\rangle$. We identify $\langle |E_\omega(x_1,z)|^2\rangle c$ as the field intensity $I(x_1,z)$, where c is the speed of light.

Determining the field intensity and coherence function requires performing a double summation over all possible eigenfunctions of the spectrum, cf. Eq. (9). The inherent non-self-adjoint nature of the transverse operator [Eq. (4)] implies that the off-diagonal contributions in Eq. (9) are nonzero in general and that the diagonal terms satisfy $\int|u_n|^2dx/\int u_n^2dx>1$. The left-hand side of this latter inequality defines the Petermann factor, which has served as a conventional measure of the amount of excess spontaneous noise arising from each eigenfunction [12]. However, this definition makes no allowances for cross-correlation effects between differing eigenmodes, which can greatly modify the amount of excess spontaneous noise up to moderate values of the gain-length product. For systems dominated by only one laser mode, the Petermann factor provides a meaningful description of excess noise. However, present ASE experiments do not seem to be dominated by one transverse mode but by many modes, some of which are marginally bound and may indeed contribute substantially to the excess noise level. In this case the effect of cross-correlations between eigenmodes may significantly reduce the level of excess noise as gauged by the Petermann factor. We now illustrate this phenomenon by studying in detail the case of a transverse square gain profile.

B. Square transverse gain modeling: The spectrum

We consider the following square gain and refraction profiles:

$$g(x,\omega)=\begin{cases} g_0 & \text{if } |x|\le 1 \\ 0 & \text{if } |x|>1\ , \end{cases} \tag{13a}$$

$$h(x)=\begin{cases} h_0 & \text{if } |x|\le 1 \\ 0 & \text{if } |x|>1 \end{cases} \tag{13b}$$

for a finite slab geometry of half-width $A>1$ (see Fig. 2). The finite geometry is employed only as a mathematical device to naturally introduce the continuum; no physical significance is necessarily attached to the actual location of the boundaries. The ensuing analysis will bear a close relationship with the well-known quantum-mechanical treatment of a square well or barrier, but where the gain now acts as a potential well and the refraction strength behaves as a potential barrier. Similar modeling has previously been applied toward simple diode junction lasers, with transverse intensity profiles generally dominated by far fewer modes than for the case of an ASE x-ray laser [19]. From the former application, the phenomenon of excess noise was later predicted, but only within the context of the fundamental laser mode [12]. Here we are interested in exploring this phenomenon for the case of *all* laser modes which pertains to an x-ray laser.

The square transverse profiles considered here are not proposed as realistic descriptions of a laboratory ASE x-ray laser medium. There are two main reasons why we choose to use these simple transverse profiles as given by Eqs. (13a) and 13(b). First, an understanding of some key properties of excess noise in an ASE x-ray laser is greatly advanced by adopting such a simple model. Second, the consideration of more realistic profiles can be conveniently based on the relatively simple properties of the square transverse profile as a starting point. In a forthcoming paper we will show that the derived properties of the square transverse profile prove useful in studying arbitrary profiles by simply numerically evolving the square case into any desired configuration.

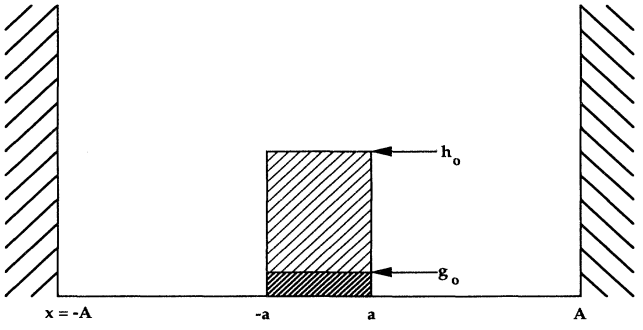

FIG. 2. Geometry of lasing medium with outer conducting boundaries.

We adopt perfectly reflecting boundary conditions at $x=\pm A$ so that $E_\omega(x)$ is vanishing at both boundaries. The eigenfunctions are of two types: even and odd parity. For example, the even parity solutions to the paraxial wave equation (4) read

$$u_n(x)=N_n\begin{cases}\cos\beta_n x+D_n\sin\beta_n x, & x>1\\ A_n\cos\alpha_n x, & |x|\le 1\\ \cos\beta_n x-D_n\sin\beta_n x, & x<1\end{cases} \tag{14}$$

where $\beta_n=-\sqrt{E_n}$, [20], $\alpha_n=[\beta_n^2-F_e(\eta-i)]^{1/2}$, N_n is the normalization constant, and A_n and D_n are determined by matching conditions on $u_n(x)$ and $du_n(x)/dx$ at $x=1$:

$$D_n=\frac{\beta_n\tan\beta_n-\alpha_n\tan\alpha_n}{\alpha_n\tan\beta_n\tan\alpha_n+\beta_n}\ , \tag{15}$$

$$A_n=\frac{\beta_n}{\alpha_n\sin\alpha_n\sin\beta_n+\beta_n\cos\alpha_n\cos\beta_n}\ . \tag{16}$$

The vanishing of E_ω at $x=\pm A$ determines the eigenvalue condition

$$\alpha_n\tan\alpha_n=\beta_n\cot[\beta_n(A-1)]\ . \tag{17}$$

We divide the spectrum into two distinct types: discrete or bound modes and continuum or free modes, in analogy with quantum-mechanical potential theory. The bound modes are determined from the condition that $\mathrm{Im}(\beta_n)>0$ remain finite in the limit as $A\to\infty$. This ensures that the bound eigenfunctions are localized near the lasing medium and tend asymptotically to zero with increasing A. For the bound even parity solutions the eigenvalue condition (17) reduces to

$$\alpha_{nb}\tan\alpha_{nb}=-i\beta_{nb}\ , \tag{18}$$

where the nb subscript is used to distinguish the bound-mode portion of the spectrum. For $\mathrm{Im}\beta_{nb}>0$, the solutions of Eq. (18) yield a finite set of eigenvalues that was treated previously by London, Rosen, and Strauss [5]. For typical x-ray laser experimental parameters, both $F_e\gg 1$ and $F_e/\eta\gg 1$ are satisfied [1,21], and the number of bound or guided eigenmodes n_g scales as $2F_e/\{\pi\ln[F_e/(1+\eta)]\}$ [5]. Typically, n_g is on the order of several hundred, which is merely an artifact of the sharp-edged profiles we have chosen. For more realistic profiles that are smooth everywhere, e.g., $g(x,\omega)$, $h(x)\propto\mathrm{sech}^2(x/a)$, the number of bound states can be shown to be on the order of only five–ten [5]. In general, the spectrum is misrepresented by including only the bound or guided modes in the low and intermediate gain-length regime; the continuum modes must also be considered, as we verify shortly.

The free or continuum modes (denoted by the subscript E) are defined by the requirement that in the limit as $A\to\infty$, the product $A\,\mathrm{Im}(\beta_E)\equiv\kappa_E$ remain finite or at most scales logarithmically with A. Stated more simply, the free modes remain finite in x as $A\to\infty$. Analytic properties of the continuum modes are presented in Appendix A.

The solutions of the transcendental eigenvalue equation (17) are readily found by the Newton-Raphson root-finding technique. Figure 3 displays a particular spectrum of even-parity eigenmodes in the complex-β plane. Shown also is the contribution to the spectrum from the bound or discrete modes. The first bound mode appears precisely at the top of the refractive "potential' barrier, i.e., $\mathrm{Re}(-\beta_{nb})=(F_e\eta)^{1/2}$, with successive bound modes found above the barrier. The last bound mode nearly merges with the continuum, indicating a virtual coalescence of the two branches of the spectrum in this region of the β plane. It is quite clear that situations may arise in which this last marginally bound mode is practically indistinguishable from its neighboring set of continuum eigenstates. This possibility nicely illustrates the need to include the contribution from neighboring free modes when considering the field intensity associated with a loosely bound mode.

A further look at Fig. 3 shows that the presence of bound modes in the spectrum has the effect of locally perturbing the underlying continuum states upward [in $\mathrm{Im}(\beta)$], particularly those near the more loosely bound modes. Beyond the last bound mode, however, the continuum continues to experience a similar type of behavior, despite the apparent absence of bound states. We can gain some insight into this phenomenon if we briefly note that the $A=\infty$ analysis of London, Rosen, and Strauss [5] happens to also generate unbounded (in x) solutions that very nearly coincide in $\mathrm{Re}(-\beta)$ with the positions of the local maxima of the continuum in Fig. 3. These spurious solutions (or negative energy states) were correctly discarded on physical grounds in their analysis, but the effect of these quasimodes on our finite A model is unmistakable: free-state resonances arise in their place instead [22]. Such resonant states have their natural analogue in quantum mechanics, where free states in the vicinity of a transmission resonance can behave as "almost bound states" in a potential well [23]. As we demonstrate in the next section, the spectrum associated with any ASE medium can be approximately viewed as an infinite set of "normal" modes that consists of a finite number of bound modes and a complementary set of "almost-bound states" or resonances originating from the

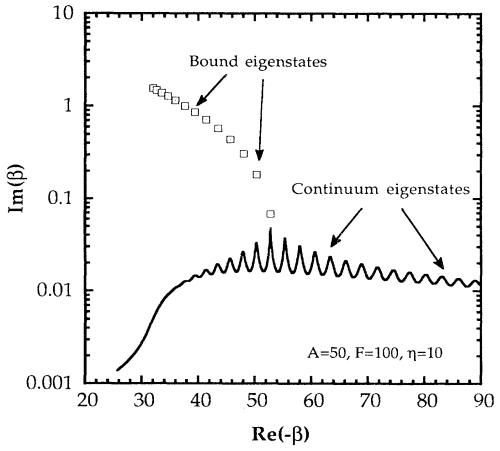

FIG. 3. Spectrum of even-parity eigenmodes in complex eigenvalue (β) plane.

continuum. However, weakly bound modes and neighboring free-state resonances are not at all independent but effectively interact to give a substantially reduced intensity contribution. This simplified description of the spectrum may prove useful for more complicated gain and refraction strength profiles, which may effectively prevent us from performing a detailed spectral analysis.

C. Square transverse gain modeling: The intensity

An understanding of the spectrum for Eq. (4) now allows us to consider in some detail the properties of intensity profiles in an ASE transverse square gain medium. We begin by rewriting Eq. (9) for the correlation function in terms of explicit bound and continuum contributions:

$$\langle E_\omega(x_1,z)E_\omega^*(x_2,z)\rangle = C_1\left[\sum_{n,m} B_{n,m}u_n(x_1)u_m^*(x_2)(e^{iz(E_n-E_m^*)/2}-1)+\sum_{E,E'} B_{E,E'}u_E(x_1)u_{E'}^*(x_2)(e^{iz(E-E'^*)/2}-1)\right.$$
$$\left.+\sum_{n,E} B_{n,E}u_n(x_1)u_E^*(x_2)(e^{iz(E_n-E^*)/2}-1)+\sum_{E,n} B_{E,n}u_E(x_1)u_n^*(x_2)(e^{iz(E-E_n^*)/2}-1)\right], \tag{19}$$

where the first expression on the right-hand side represents the bound-bound (b-b) contribution, the second term is the free-free (f-f) portion, the third term refers to the bound-free (b-f) contribution, the last expression corresponds to the free-bound (f-b) portion of the electric-field correlation function, and the $B_{i,j}$'s are defined below Eq. (11). For ease of notation we have replaced the previous bound-mode subscript nb by the subscript n in Eq. (19).

In this section we concentrate on analytically evaluating Eq. (19) for the integrated intensity to see to what degree the intensity contribution from free modes can cancel the anomalously large intensity associated with one marginally bound mode. Setting $x_1=x_2$ and integrating Eq. (19) over x_1 for the total intensity $I_{\rm tot}$ gives with the aid of Eq. (6)

$$I_{\rm tot}(z)=\left[\frac{cC_1}{8\pi}\right]\left[\sum_{n,m} B_{n,m}^2(e^{iz(E_n-E_m^*)/2}-1)\right.$$
$$+\sum_{E,E'} B_{E,E'}^2(e^{iz(E-E'^*)/2}-1)$$
$$+\sum_{n,E} B_{n,E}^2(e^{iz(E_n-E^*)/2}-1)$$
$$\left.+\sum_{E,n} B_{E,n}^2(e^{iz(E-E_n^*)/2}-1)\right], \tag{20}$$

where

$$B_{i,j}=\frac{F_e N_i N_j^* A_i A_j^*}{[\frac{i}{2}(E_i-E_j^*)]}\left[\frac{\sin(\alpha_i-\alpha_j^*)}{(\alpha_i-\alpha_j^*)}\pm\frac{\sin(\alpha_i+\alpha_j^*)}{(\alpha_i+\alpha_j^*)}\right], \tag{21}$$

i and j both refer to bound or free states, the $+$ ($-$) sign denotes even (odd) parity eigenfunctions, and the coefficients A_i are determined from Eq. (16). For large half-width A, the normalization constants for the bound and free states are readily evaluated:

$$N_n=\left[A_n^2\left[1\pm\frac{\sin 2\alpha_n}{2\alpha_n}\right]-\frac{e^{2i\beta_n}}{2i\beta_n}\right]^{-1/2}, \tag{22}$$

$$N_E=[A(1+D_E^2)]^{-1/2}. \tag{23}$$

We can make further use of the large A assumption by converting the sums over free states in Eq. (20) into integrals over β_{E1}:

$$\frac{1}{A}\sum_E \rightarrow \frac{1}{\pi}\int_{-\infty}^{0} d\beta_{E1}. \tag{24}$$

Consider two neighboring marginally bound modes in Eq. (20), which we label with the indices n' and m'. We wish to estimate the intensity derived from these particular bound modes, taking into account the effect of neighboring or "resonant" free modes. Clearly, the diagonal elements ($n=n'$, $m=m'$) in the b-b summation of Eq. (20) will dominate this partial contribution to the total intensity if $\mathrm{Im}(\beta_{n'})$ and $\mathrm{Im}(\beta_{m'})$ are small relative to those of the other bound modes. For the other three terms in Eq. (20) involving free-mode contributions, i.e., f-f, b-f, and f-b, we note that their contribution is only dominant in the vicinity of a bound mode, i.e., when $E\approx E_{n'}$ and $E'\approx E_{m'}$. This simply follows from Eq. (23), where a resonance is identified for $D_E=\pm i$. However, with use of Eqs. (15) and (18), this condition defines precisely the bound-mode dispersion relation, Eq. (18). Thus, we may Taylor expand all of the exponential terms in Eq. (20), noting that this procedure holds even for quite large values of the gain-length parameter $g_0 z$ if the mode is very marginally bound and $n'=m'$. This means that our analysis is not necessarily restricted only to the spontaneous-emission stage ($g_0 z<1$), where no gain discrimination of modes occurs.

In the vicinity of one loosely bound mode (labeled by n) we may evaluate Eq. (20) by contour integration methods, which are briefly described in Appendix B. The various intensity contributions are found to satisfy

$$I_{b\text{-}b}^{(n)}=I_{f\text{-}f}^{(n)}=-I_{b\text{-}f}^{(n)}=-I_{f\text{-}b}^{(n)}. \tag{25}$$

Equation (25) clearly demonstrates that the total intensity

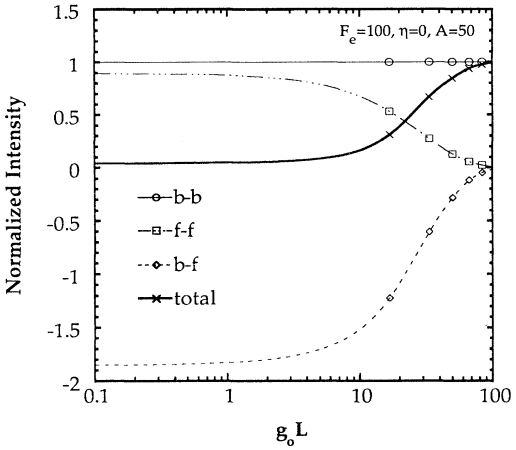

FIG. 4. Dispayed are the normalized integrated intensity contributions from the bound-bound (b-b), free-free (f-f), bound-free plus free-bound (b-f) terms in Eq. (20) and their sum (total) as a function of gain-length parameter g_0L in the absence of refraction ($\eta=0$).

$I_{\text{tot}}=I_{b\text{-}b}+I_{f\text{-}f}+I_{b\text{-}f}+I_{f\text{-}b}$ vanishes in the spontaneous-emission stage. Figure (4) displays the relative contributions to the total intensity for a particular weakly bound mode ($\text{Re}\beta_{n'}=27.4$, $\text{Im}\beta_{n'}=0.118$, $\text{Im}(E_{n'}/F_e)=g_{n'}/g_0=0.065$, $A=50$), which were found by numerically evaluating Eq. (20). In this evaluation we sum over the free modes (≈ 50) in the immediate vicinity of the bound mode on the $\text{Re}(-\beta)$ axis (see Fig. 3). Strong confirmation of our analysis is evident even for gain-length parameters a good deal larger than unity. The conclusion drawn from this exercise is that the intensities derived from loosely bound modes make little global contribution to the total intensity for small and moderately large gain-length parameters. Thus the "excess noise" derived from marginally bound modes is insignificant in the presence of cross-correlation effects. For larger gain-length parameters, gain discrimination renders irrelevant any contribution from loosely bound states, since the higher gain states (or more tightly bound states) dominate the intensity. In the next section we study the amount of cancellation occurring in the local intensity.

III. INTENSITY AND COHERENCE PROFILES

A. Intensity

The evaluation of the average ASE intensity profile from Eq. (19) (with $x_1=x_2$) is analytically intractable in general and requires a numerical effort. In this section we examine further the role of excess noise on ASE intensity profiles by verifying the local cancellation of b-b intensities, qualitatively studying the degree of spectral completeness, and determining total intensity profiles for experimentally relevant gain-length parameters.

1. Local b-b intensity cancellation

In the last section we confirmed that the anomalously large contributions from loosely bound modes to the spatially integrated intensity disappear within the context of a complete spectrum, at least in a global sense. Figure 5(a) shows the various intensity contributions as a function of transverse position. A particular loosely bound (odd-parity) mode with the same parameters as used in Fig. 4 and which has an appreciable amplitude well away from the lasing slab ($|x|\leq 1$) was selected. The neighboring free modes were chosen with the aid of Fig. 3 by selecting only those modes situated near a local maximum in $\text{Im}(\beta)$ that also coincides with the bound mode under consideration. The results are not at all sensitive to the precise segment of the continuum used as long as the few free modes lying near the center of the resonance are included. Although the individual component intensities are relatively large over the transverse distance indicated, the total intensity profile shows how effective the cancellation is almost everywhere. Beyond $x\approx 3$, the global cancellation rule represented by Eq. (25) turns out to be quite well obeyed for this local case. As we increase the parameter g_0z, the b-b component of intensity in-

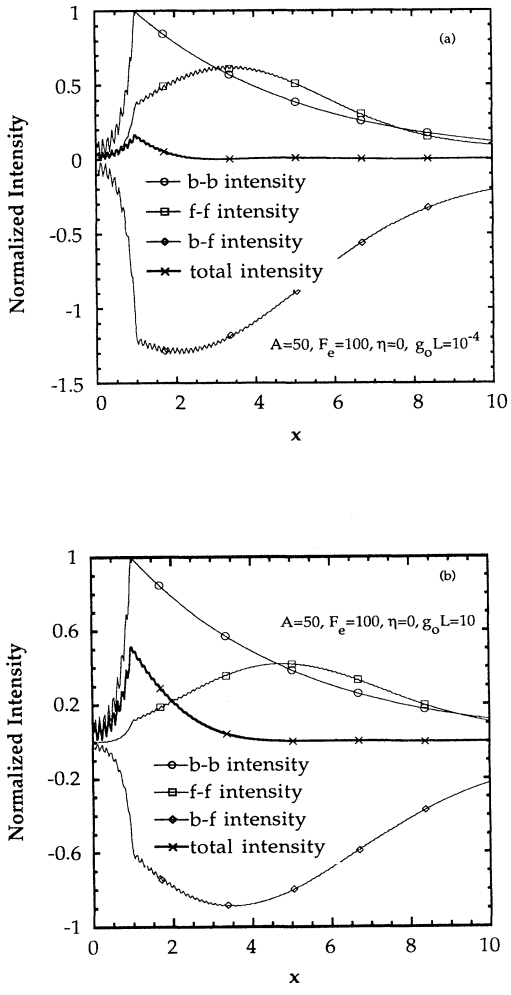

FIG. 5. Shown are the normalized local intensity contributions from the bound-bound (b-b), free-free (f-f), bound-free and free-bound (b-f) terms in Eq. (19) (with $x_1=x_2$) vs normalized transverse position x for gain-length $g_0L=10^{-4},10$.

creases, but as Fig. 5(b) demonstrates, significant cancellation still occurs even for $g_0 z$ as large as 10.

2. Spectral completeness

As we have indicated in Sec. II A, the issue of spectral completeness is very relevant to our use of the modal approach in exploring the degree to which excess noise phenomena may affect our conceptual understanding of ASE x-ray laser intensity and mutual coherence profiles. So far we have exhaustively examined many aspects of a square gain profile under the working assumption that our spectrum of normal modes is "adequately" complete. A precise measure of completeness is beyond the scope of this paper, but we can gain some insight into a qualitative measure of this property by analyzing intensity profiles in the very low gain-length parameter regime.

In the limit $z \rightarrow 0$, Eq. (9) for the field correlation function becomes

$$\langle E_\omega(x_1,z)E_\omega^*(x_2,z)\rangle = z\sum_{n,m}\left[\int_{-\infty}^{\infty} dx\,dx'\langle P_{\rm sp}(x)P_{\rm sp}^*(x')\rangle u_n(x)u_m^*(x')\right] \times u_n(x_1)u_m^*(x_2)\ , \quad (26)$$

where we have relaxed the previously assumed form of the spontaneous-emission correlation function, Eq. (10), as follows:

$$\langle P_{\rm sp}(\mathbf{r}_1)P_{\rm sp}^*(\mathbf{r}_2)\rangle \rightarrow \delta(z_1-z_2)\langle P_{\rm sp}(x_1)P_{\rm sp}^*(x_2)\rangle\ . \quad (27)$$

For a biorthonormal basis set, spectral completeness is defined by the relation [9]

$$\sum_n u_n(x_1)u_n(x_2)=\delta(x_1-x_2)\ . \quad (28)$$

Applying Eqs. (26)–(28) and performing the integrations gives

$$\langle E_\omega(x_1,z)E_\omega(x_2,z)\rangle = z\langle P_{\rm sp}(x_1)P_{\rm sp}^*(x_2)\rangle\ . \quad (29)$$

Physically, a minimum correlation length for spontaneous emission should be on the order of an atomic dimension [10]. Accounting for such a correlation length allows us to take $x_1=x_2$ for evaluating the intensity without formally encountering a divergence, cf. Eq. (10).

An important feature of Eq. (29) is that the right-hand side must vanish where the density of spontaneous emitters is zero and that the field intensity within the gain medium must be flat, since the density of upper-state emitters N_2 is assumed constant in x. More simply stated, the intensity profile must reproduce the source profile if the spectrum is complete [9]. Consequently, a qualitative measure of completeness is found by comparing a computed transverse intensity profile for a given basis set of eigenfunctions with this idealized field profile. In Fig. 6 we display some intensity profiles as a function of the number of eigenmode states n_β (free and bound) that are taken to define a basis set. For larger values of n_β, the source is satisfactorily reproduced by the profiles, although some slight difference with the idealized case is

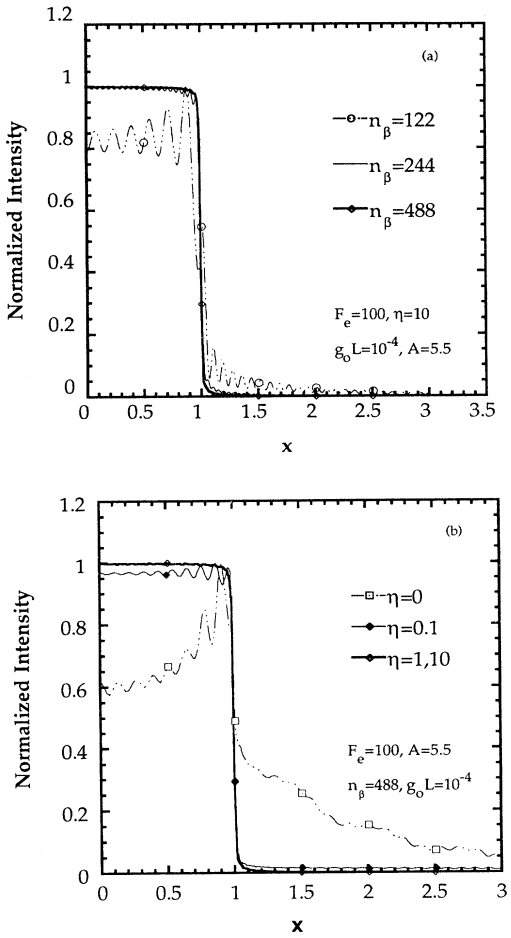

FIG. 6. (a) Normalized local intensity vs transverse coordinate x for three spectra labeled by the total number n_β of modes included, and (b) normalized local intensity vs normalized transverse coordinate x for two values of the refraction strength parameter η.

evident. A quantitative measure of the discrepancy is a difficult endeavor, but a qualitative notion of completeness can be gleaned from inspection of very low gain-length intensity profiles in general. Figure 6(b) displays two intensity profiles that differ only in the value of the refraction strength parameter η. Clearly, the $\eta=1$ and 10 cases do a better job of reproducing the source for the same number of free modes compared to the lower η examples. We note that as η becomes large compared to one, the "potential" term in Eq. (4) is nearly real and the eigenvalue problem is approximately Hermitian with respect to the continuum portion of the spectrum. On the basis of conventional perturbation theory arguments [24], the degree of completeness can therefore be quantified, since the spectrum is dominated by the continuum in the low gain-length regime. However, for $\eta=0$, the "potential" term is strongly non-Hermitian (or actually anti-Hermitian), so that the gain cannot be treated as a perturbation. Thus, we are not able to say to what degree the spectrum is possibly incomplete in the absence of refraction. For present ASE x-ray laser exper-

iments, the refraction parameter η typically exceeds 50, and the issue of spectral completeness fortunately does not appear to be of serious concern.

3. *Spectral cutoff*

A major issue raised by Eq. (29) is the possible divergence of the field energy when the spontaneous-emission correlation length goes to zero. This feature requires the introduction of a spectral cutoff, several of which we now consider. A plausible lower limit for the correlation length is of the order of an atomic dimension [10], but for the physical examples in mind an atomic scale length is very small compared to the transverse extent of the laser. With use of Eqs. (A1) and (A3) we can estimate the number of modes corresponding to this cutoff: $n_\beta \sim k_c A/\pi$, where k_c represents a transverse wave-vector cutoff or a reciprocal correlation length (times 2π) for spontaneous emission. Consequently, the number of off-diagonal elements ($\sim n_\beta^2$) involved in the calculation of the total field intensity can become prohibitively cumbersome for realistic x-ray laser parameters ($F_e \sim 10^3$, $g_0 a \sim 0.05$, $k_c/k \sim 10$, $ka \approx 3\times 10^4$, $a \approx 100$ μm, and $A/a > 5$, giving $n_\beta > 10^6$). The validity of the paraxial approximation naturally demands an upper limit on the propagation angles of the radiation with its associated cutoff $n_\beta \sim (A/a)F_e/(\pi g_0 a)$, but this is still inaccessibly large in general. A further constraint may be found by equating the spontaneous-emission rate $\hbar\omega N_2 \gamma_R V/3$ to the (transversely) integrated intensity $\int I(x,z)dx\,dy$, where V is the lasing volume and γ_R is the radiative relaxation rate. With the aid of Eqs. (9), (11), (A1), (A5), and (24), we can estimate the following maximum value of β: $\beta_{\max} \sim k/(24\pi)$. Here we have assumed that the field intensity is flat and localized to the lasing medium ($|x| \le 1$) and that the higher free modes are mutually orthogonal. From Eqs. (A1), (A3) we can further show that the corresponding total number of free modes is on the order of several hundred for $kA = 1.5\times 10^5$ ($k = 3\times 10^6$ cm^{-1} for neon-like Se, $A = 5.5a \approx 550$ μm), which agrees well with the maximum number of free modes used for Figs. 6(a) and 6(b). This represents a dramatic improvement over the previous constraints described above, but the criterion does not take into account gain discrimination effects for larger values of gain-length product, which is our primary interest. For this purpose the Fresnel number for one transverse dimension is particularly convenient and arises naturally by including only those rays that have *not* undergone a reflection at the boundary: $k_\perp/k \le A/L$, where L is the length of the laser. In terms of the free modal index n, we can rewrite this condition with the aid of either of Eqs. (A1) or (A3):

$$n \cong \frac{F_e}{g_0 L}\left[\frac{A}{a}\right]^2 \frac{1}{\pi}, \tag{30}$$

which serves as a rough, yet useful, estimate of the number of free modes (of either parity) to consider. The physical motivation for this nonreflecting constraint is that the dominant laser modes that are observed are not expected to have undergone one or more reflections, since the associated trajectory would yield very minimal amplification. This argument is not at odds with our mathematically imposed reflecting boundary condition [see below Eq. (13b)] because the boundaries at $x = \pm A$ are imposed not as a realistic feature of a laser, but only as a mathematical aid to allow us to define and normalize the eigenfunctions. Physically, we would prefer to let $A \to \infty$, but as A increases, more continuum states arise, and a numerical evaluation of the electric-field correlation function [Eq. (9)] becomes quite impractical.

Still another constraint, though more stringent than the nonreflecting constraint, is that waves with trajectories lying principally within the gain medium be selected only, i.e., $k_\perp/k \le 2a/L$, or, in terms of the number of free modes (of either parity),

$$n \cong \frac{2}{\pi}\frac{F_e}{g_0 L}\frac{A}{a}. \tag{31}$$

The choice between Eq. (30) or (31) as a cutoff for the spectrum is largely arbitrary. The overall ambiguity in deciding on a spectral cutoff encountered here basically arises because the underlying assumption used in our treatment is that the source term $\langle P_{\rm sp} P_{\rm sp}^* \rangle$ excites *equally* all of the eigenmodes, with no discrimination occurring under our adopted choice of boundary condition. In the next section we concentrate on using Eq. (30) as our adopted spectral cutoff.

4. *Intensity profiles for moderate $g_0 L$*

We now examine the intensity profiles in the intermediate gain-length regime. Previously, London, Rosen, and Strauss have computed intensity profiles in this relevant experimental regime and found an unacceptable sensitivity on the value of gain strength for small gain lengths and large values of F_e [5]. We now redo some cases with the free modes included and study their overall effect. Figures 7(a) and 7(b) display the *b-b* intensity profiles and total intensity profiles when both constraints on the free-mode spectrum, Eqs. (30) and (31), are used [25]. A significant difference between the total intensity profile and the *b-b* profile is seen in Fig. 7(a) with $g_0 L = 5$, particularly when the cutoff described by Eq. (31) is used. As we increase the refraction strength parameter as in Fig. 7(b), the relative contribution from the free-mode portion of the spectrum, i.e., *f-f* + *b-f* + *f-b*, remains significant for the same cutoff.

We now settle on exclusively using Eq. (30) to constrain the free-mode spectrum. In Figs. 8(a) and 8(b), we plot the *b-b* and total intensity profiles for both $g_0 L = 5, 10$. For the case of $\eta = 0$, the free-mode contribution to the intensity is very slight at higher $g_0 L$, and barely perceptible in the presence of refraction ($\eta = 10$), Fig. 8(b). Thus, we can conclude that the issue of spectral cutoff is important for moderate values of gain length; for higher $g_0 L$, the effect of gain discrimination renders the free-mode contribution practically irrelevant.

London, Rosen, and Strauss have noted in their analysis a disturbing sensitivity of the *b-b* intensity profile outside of the gain medium ($|x| \le 1$) on the strength of the gain g_0 [5]. From further inspection of Fig. 8(a) we

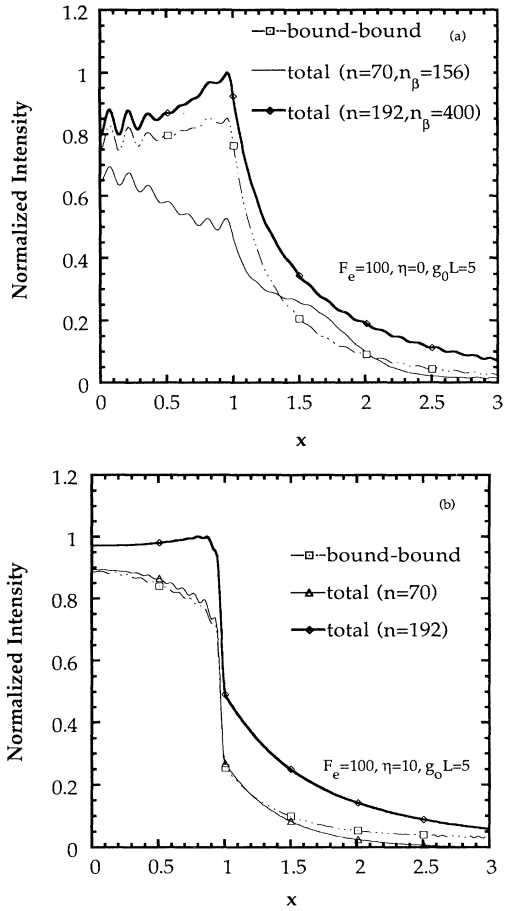

FIG. 7. Normalized local intensity vs normalized transverse position x for three types of spectra with no refraction (a) and with refraction (b). The variable n refers to the number of free modes included in the (total) spectrum as determined by Eqs. (30) and (31).

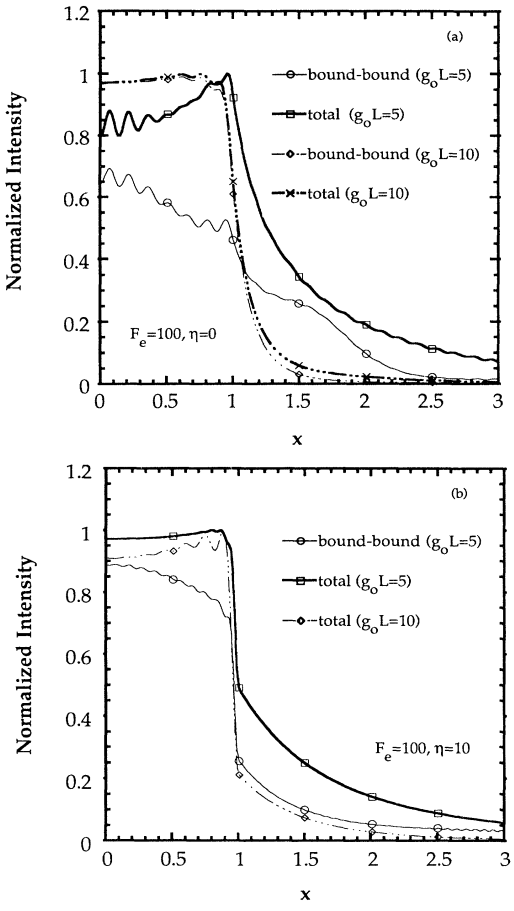

FIG. 8. Normalized local intensity vs x for two values of the gain-length parameter with no refraction (a) and with refraction (b). The indicated spectra include bound modes only (bound-bound) and bound modes plus free modes (total), according to Eq. (30).

do notice some surplus *b-b* intensity outside of the slab, but not a large amount of anomalous energy. The explanation for this reduced noise is that the finite geometry model we are considering, i.e., finite A, effectively truncates the higher end [in $\mathrm{Re}(\beta_n)$] of the bound-mode spectrum and transforms the very loosely bound modes into free modes. Thus, the modes responsible for large "excess noise" found in the $A=\infty$ analysis of London, Rosen, and Strauss [5] are practically forced into the continuum of our finite A model, where their intensity contribution largely cancels. For large values of A, the integrity of the bound modes is well maintained vis-à-vis the free modes. However, for the relatively small value of $A\,(=5.5)$ employed in Figs. 7 and 8, the distinction between a loosely bound mode and a free mode essentially disappears. In this case we must be careful to concentrate on summing over *all* the modes without dwelling on what to label the various "divisions" of the full spectrum. For the sake of convention only, we settle on characterizing those modes that have direct correspondences [in $\mathrm{Re}(-\beta)$] with the guided modes found in the $A=\infty$ analysis of London, Rosen, and Strauss [5] as bound modes despite their hybrid nature in the small A case.

Figure 9 displays the total intensity profiles from three separate models for describing ASE x-ray laser properties: (1) our finite geometry modal analysis, (2) the unbounded model of London, Rosen, and Strauss [5] and (3) a time-dependent numerical wave optics propagation treatment by Feit and Fleck [26]. First, a large difference between our *b-b* intensity profile and the total intensity profile of London, Rosen, and Strauss (which includes only bound modes) is very evident. In particular, the intensity profile of London, Rosen, and Strauss shows a significant portion of energy beyond $x=1$, which is due to uncompensated loosely bound modes or "excess noise." Second, the total intensity profiles derived from our model and the analysis of London, Rosen, and Strauss show substantial differences over most of the range of x for this intermediate value of g_0L. However, as we increase g_0L beyond about ten, the two profiles become essentially indistinguishable because of gain

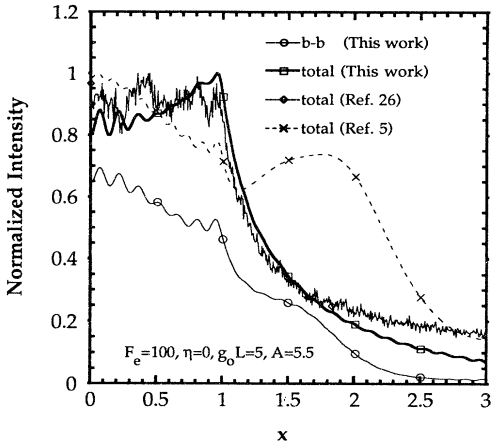

FIG. 9. Normalized intensity profiles for four different models with no refraction. The indicated spectra derived from our model include bound modes only (*b-b*) and bound modes plus free modes (total), according to Eq. (30).

discrimination and the decreased importance of cross-correlation effects. Although cross-correlations have substantially degraded the intensity contribution from loosely bound modes, there still persists an excess noise (or Petermann) factor associated with the dominant modes that has recently been experimentally verified [27]. Also evident from Fig. 9 is the relatively good agreement between our total intensity profile and the predicted intensity from Feit and Fleck. Although we defer an exhaustive comparison of the two approaches to a later publication, we can say that the agreement is reassuring in view of the very different nature of the two methods.

B. Coherence

An understanding of the coherence properties of ASE x-ray lasers is of crucial importance for their eventual application to holography. London, Rosen, and Strauss have investigated coherence phenomena from the point of view of optimization. They concluded that rounded profiles, such as parabolic, provide acceptable coherence when the lasing medium width is suitably, but not unreasonably, small. For square gain profiles, the number of bound modes is substantially larger, thereby degrading the degree of coherence to an unacceptable level. Coherence is always improved in the far field, but the resulting low level of energy deposition is the serious tradeoff. Because our present analysis is restricted to the special case of square profiles, we cannot reliably address the specific issue of laboratory x-ray-laser coherence; rather, we intend to explore qualitatively the influence of the free-mode portion of the spectrum on the amount of noise that survives and its effect on coherence, using Eq. (12). As found in Sec. III A 4 in our study of intensity profiles, we expect some significant effects for intermediate values of the gain-length parameter.

Figure 10(a) shows the coherence profiles for the *b-b* portion of the spectrum and the "full" spectrum, which includes the free-mode contribution as constrained by

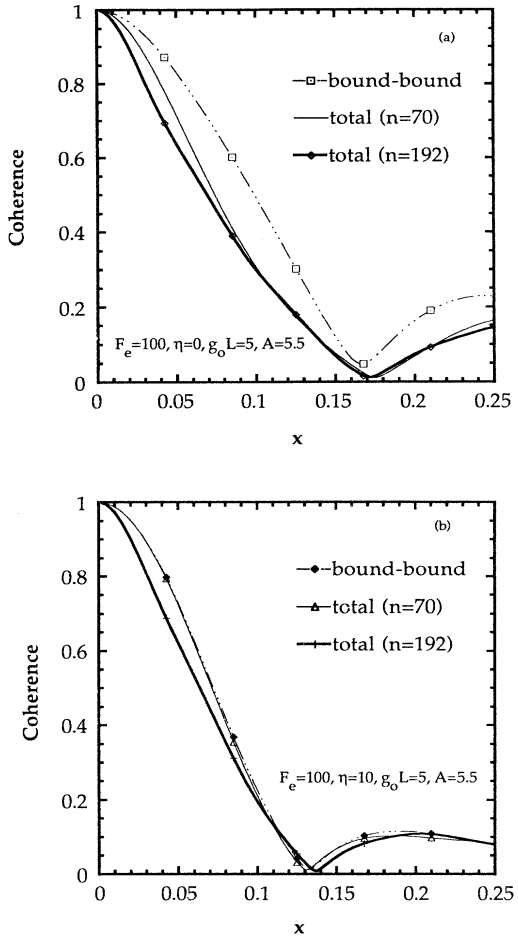

FIG. 10. Coherence profiles for three separate spectra with no refraction (a) and with refraction (b). The variable n refers to the number of free modes included in the spectrum, (total), according to Eqs. (30) and (31).

Eqs. (30) and (31). Clearly, the addition of more free states [as given by Eq. (30)] degrades the coherence significantly in the absence of refraction. In Fig. 10(b) refraction is seen to lessen the effects of the continuum: both total coherence profiles are in close proximity to the *b-b* profile. Figure 11(a) shows the effect of increasing gain length on the free-mode contribution to the total coherence. Beyond $g_0L \sim 10$, the total coherence properties are dominated by the most localized bound modes and "excess noise" is not an important factor. For nonzero refraction strength, the same conclusion holds, as shown in Fig. 11(b). The overall decrease in coherence evident in Fig. 11(b) is due to the general increase in the number of bound modes n_g as the refraction strength parameter η is increased. The slow increase with η of n_g is due to internal reflections from the sharp boundaries at $x = \pm a$, which are not realistic features of a plasma x-ray laser but may be applicable to hard-edged lasers.

Finally, in Fig. 12 we compare the various coherence profiles from our analysis and the models of London, Rosen, and Strauss [5] and Feit and Fleck [26]. The de-

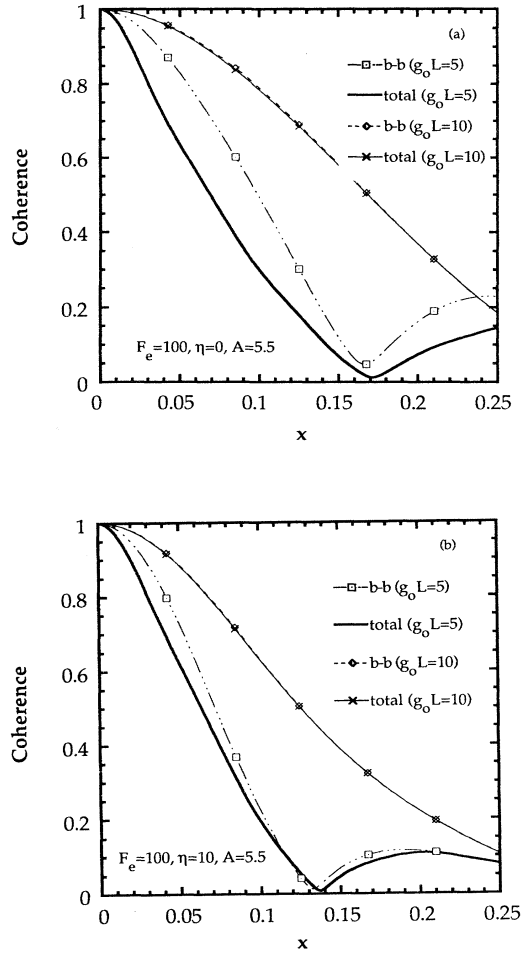

FIG. 11. Coherence vs x for two values of the gain-length parameter with no refraction (a) and with refraction (b). The indicated spectra include bound modes only (bound-bound) and bound plus free modes (total), as constrained by Eq. (30).

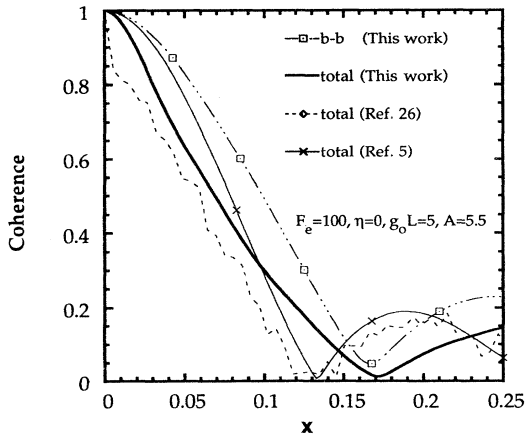

FIG. 12. Coherence profiles for four different models with no refraction. The indicated spectra obtained from our model include bound modes only (*b-b*) and bound modes plus free modes (total), according to Eq. (30).

gree of spatial coherence is often measured by the coherence length, which is defined as the distance over which the coherence profile falls to some number typically between 0.5 and 0.85. From inspection of Fig. 12 we note that our *b-b* coherence profile is somewhat better than the coherence found by London, Rosen, and Strauss. The reason is simply that a finite A analysis effectively loses the most marginally bound modes to the continuum. With fewer bound modes remaining, the field coherence can only improve. Overall, all four profiles shown are in rough agreement with each other for this specific value of gain-length parameter. The coherence predicted by Feit and Fleck is somewhat poorer than the other profiles shown. This may be attributed in part to the larger spectral base ($\sim$2048 orthogonal modes) used in comparison with our nonorthogonal basis set (400 modes for this particular example). For larger g_0L, the effect of gain discrimination will yield rapid convergence among the four different profiles.

IV. SUMMARY

The previous square gain analysis by London, Rosen, and Strauss has provided evidence of a peculiar sensitivity of the intensity and coherence profiles on the precise strength of the gain parameter g_0, which is a manifestation of the "excess noise" phenomenon. For small and intermediate values of the gain-length parameter, this effect can be particularly prominent. The point of this paper has been to remove this anomaly by considering the role of the free modes on the spectrum through cross-correlation effects, thereby greatly reducing the level of excess noise in the system. We emphasize that not all of the excess noise is removed from the system in this manner: what surplus noise remains is aptly described by the Petermann factor for the most dominant modes.

We have limited our study to the case of square gain and density profiles mainly for analytic ease. However, a thorough study of this basic profile is essential to understanding from a modal viewpoint the role of potentially high noise levels in ASE systems. Our goal has been to extract as many salient features as possible from this analysis with the idea of applying these insights toward more realistic but less tractable profiles. In particular, the sharp corners of a square profile yield some modal features somewhat distinct from those of smooth profiles. Consequently, we cannot yet view our modal treatment as a phenomenological model for understanding many properties of current ASE x-ray laser experiments. We expect that our future investigations with smooth profiles will provide more direct relevance for x-ray laser coherence experiments.

ACKNOWLEDGMENTS

We are grateful to Mordecai Rosen for stimulating discussions and to Mike Feit and Joe Fleck for the use of their WAVE code. This work was performed under the auspices of the U. S. Department of Energy by the Lawrence Livermore National Laboratory under Contract No. W-7405-ENG-48.

APPENDIX A

We derive some analytic properties of the continuum by distinguishing between three cases: (i) $\mathrm{Re}(-\beta_E) \gg (F_e\eta)^{1/2}$, (ii) $\mathrm{Re}(-\beta_E) \approx (F_e\eta)^{1/2}$, and (iii) $\mathrm{Re}(-\beta_E) \ll (F_e\eta)^{1/2}$.

Case (i): $\mathrm{Re}(-\beta_E) \gg (F_e\eta)^{1/2}$

These continuum states correspond physically to states whose "energies" lie high above the refractive "potential" barrier and are hardly affected by the presence of the lasing medium. We assume $\kappa_E \ll 1$, formally expand the even-parity dispersion relation (17) in powers of κ_E, and take the real part of α_n [which is defined below Eq. (14)] [28], to find

$$\alpha_{E1} \approx -\beta_{E1} = (n+\tfrac{1}{2})\pi/A \ , \tag{A1}$$

$$\kappa_E = -\frac{\alpha_{E2}}{\beta_{E1}} \left[\frac{\sin\alpha_{E1}\cos\alpha_{E1} + \alpha_{E1}}{\cos^2\alpha_{E1}} \right] \sin^2[\beta_{E1}(A-1)] \ , \tag{A2}$$

where α_{E1} and β_{E1} are the real parts of α_E and β_E, respectively, α_{E2} is the imaginary part of α_E, and n is an integer. For the odd-parity free modes we similarly find

$$\alpha_{E1} \approx -\beta_{E1} = n\pi/A \ , \tag{A3}$$

$$\kappa_E = \frac{\alpha_{E2}}{\beta_{E1}} \left[\frac{\sin\alpha_{E1}\cos\alpha_{E1} - \alpha_{E1}}{\sin^2\alpha_{E1}} \right] \sin^2[\beta_{E1}(A-1)] \ . \tag{A4}$$

With the aid of Eqs. (A1) and (A3) we can show that for the even (+) and odd (−) parity eigenfunctions, κ_E reduces to

$$\kappa_E = -\frac{\alpha_{E2}}{\beta_{E1}} (\pm\sin\alpha_{E1}\cos\alpha_{E1} + \alpha_{E1}) \ . \tag{A5}$$

Ordinarily, α_{E1} is much larger than unity so that $\kappa_E \approx -\alpha_{E2}$ in leading order. By considering the imaginary part of α_E, we can say further that $\kappa_E = -F_e/(2\alpha_{E1})$, which is a decreasing function of α_{E1}. Moreover, Eq. (A5) predicts that κ_E has a small-amplitude periodic variation with α_{E1} (or β_{E1}), with period $\approx\pi$.

Case (ii): $\mathrm{Re}(-\beta_E) \approx (F_e\eta)^{1/2}$

This class of continuum states has "energies" nearly matching the refractive "potential" barrier height $F_e\eta$, and the eigenvalues and eigenfunctions are strongly affected by the imaginary part of the "potential", i.e., the gain. From the real and imaginary part of α_E, we conclude that $|\beta_{E1}| \gg |\alpha_{E1}|$ and $\alpha_{E1} \approx \alpha_{E2} = (F_e/2)^{1/2}$. Again assuming κ_E to be small compared to one, using $F_e^{1/2} \gg 1$ and Taylor expanding the dispersion relations for both the even- and odd-parity solutions, we find

$$\beta_{E1} = \pi(n+\tfrac{1}{2})/(A-1) \ , \tag{A6}$$

$$\kappa_E = -(1/\beta_{E1})(F_e/2)^{1/2} \ . \tag{A7}$$

Case (iii): $\mathrm{Re}(-\beta_E) \ll (F_e\eta)^{1/2}$

These free states have "energies" lying far below the refractive "potential" barrier height and are strongly attenuated in the transverse direction within the amplifying medium. By considering the real and imaginary part of α_E we conclude that $\alpha_{E2}^2 \sim \eta F_e$ and $\alpha_{E2}/\alpha_{E1} = 2\eta$, which is typically larger than unity in practice. From the real and imaginary part of the dispersion relation we also find

$$\beta_{E1} = n\pi/(A-1) \ , \tag{A8}$$

$$\kappa_E = -\beta_{E1}/(\eta^3 F_e)^{1/2} \ll 1 \ , \tag{A9}$$

for both even and odd solutions. We further note that κ_E is an increasing function of β_{E1} in this regime.

APPENDIX B

We write the total integrated intensity in the spontaneous-emission stage as follows:

$$I_{\mathrm{tot}} = I_{b\text{-}b} + I_{f\text{-}f} + I_{b\text{-}f} + I_{f\text{-}b} \ , \tag{B1}$$

where

$$I_{b\text{-}b} = \sum_{n,m}{}' \frac{zF_{n,m}^2}{\frac{i}{2}\left[1+\frac{i}{\beta_n}\right]\left[1-\frac{i}{\beta_m^*}\right](E_n - E_m^*)} \tag{B2}$$

is the bound-bound intensity,

$$I_{f\text{-}f} = \frac{1}{\pi^2}\int_{-\infty}^{0} d\beta \int_{-\infty}^{0} d\beta' \frac{zF_{E,E'}^2}{\left[\cos^2\alpha_E + \frac{\alpha_E^2}{\beta^2}\sin^2\alpha_E\right]\left[\cos^2\alpha_{E'} + \frac{\alpha_{E'}^2}{\beta'^2}\sin^2\alpha_{E'}\right]^* \frac{i}{2}(E-E')} \tag{B3}$$

is the free-free intensity,

$$I_{b\text{-}f} = (I_{f\text{-}b})^* = \frac{1}{\pi}\sum_n{}' \int_{-\infty}^{0} d\beta \frac{zF_{n,E}^2}{\left[1+\frac{i}{\beta_n}\right]\left[\cos^2\alpha_E + \frac{\alpha_E^2}{\beta^2}\sin^2\alpha_E\right]^* \frac{i}{2}(E_n - E)} \tag{B4}$$

are the bound-free and free-bound intensities, and

$$F_{i,j}=\frac{\sin(\alpha_i-\alpha_j^*)}{(\alpha_i-\alpha_j^*)}\pm\frac{\sin(\alpha_i+\alpha_j^*)}{(\alpha_i+\alpha_j^*)} \tag{B5}$$

for even $(+1)$ and odd (-1) parity modes. Moreover, the $cC_1F_e^2/8\pi$ prefactor originating from Eqs. (20) and (21) has been ignored for convenience, the primed summation refers only to *positive* gain states ($\mathrm{Im}E_n<0$), and the $E1$ and $E1'$ subscripts on β and β' have now been dropped.

We now proceed to evaluate Eqs. (B3) and (B4) by the methods of contour integration, where β and β' are now extended from the real line into the complex β and β' planes [29]. First consider Eq. (B3), where we note that for appreciably large $\mathrm{Im}(\alpha_E)$ and $\mathrm{Im}(\alpha_E')$ on asymptotically large semicircular contours in the β and β' complex planes, respectively, the following identity holds:

$$\frac{F_{E,E'}^2}{\left[\cos^2\alpha_E+\frac{\alpha_E^2}{\beta^2}\sin^2\alpha_E\right]\left[\cos^2\alpha_{E'}+\frac{\alpha_{E'}^2}{\beta'^2}\sin^2\alpha_{E'}\right]^*}=4\left[\frac{\beta\beta'^*}{|\delta|}\right]^2\left[\frac{\alpha_E\cot\alpha_{E'}^*-\alpha_{E'}^*\cot\alpha_E}{\alpha_E^2-\alpha_{E'}^{*2}}\right]^2, \tag{B6}$$

where $\delta^2=\alpha_E^2-\beta^2=F_e(i-\eta)$. Because both $\cot\alpha_{E'}^*$ and $\cot\alpha_E\to\pm i$ on such a contour, the exponential dependence in the numerator and denominator of Eq. (B3) cancels and the contour integration is greatly simplified by dropping this contribution.

Next we locate poles of the integrands in Eqs. (B3) and (B4) and apply the residue calculus. Beside bound-mode resonances with positive gain, cf. Eq. (18), there are also resonances with negative gain ($ImE_n>0$, $\mathrm{Im}\beta_n>0$) that must be included in the evaluation. These negative-gain resonances cannot represent true physical modes since they do not satisfy Eq. (6) and therefore are not eigenfunctions of the paraxial wave equation when the medium is amplifying ($g>0$). In Fig. 13 we show a representative contour used in the evaluation of Eq. (B4) together with the indicated poles. After much analysis, we find for the total spontaneous emission

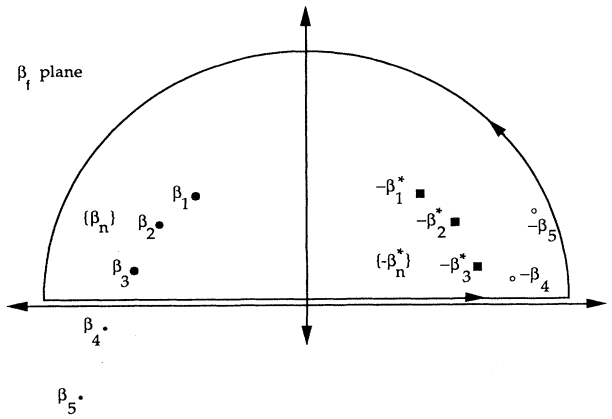

FIG. 13. Representative contour used to evaluate integral in Eq. (B4) with indicated poles.

$$I_{\mathrm{tot}}=\frac{z}{4}\left[\sum_{n,m}\frac{F_{n,m}^2}{\left[\frac{i}{2}(E_n-E_m^*)\right]}+\sum_n(\zeta_n-1)\left[\frac{F_{n,\beta_E}^2}{\beta_E\cos^2\alpha_E\left[1+\frac{\alpha_E^2}{\beta_E^2}\tan^2\alpha_E\right]}\right]_{\beta_E=\beta_n}^*-\sum_n\left[\frac{F_{n,\beta_E}^2}{\beta_E\cos^2\alpha_E\left[1+\frac{\alpha_E^2}{\beta_E^2}\tan^2\alpha_E\right]}\right]_{\beta_E=\beta_n^*}\right], \tag{B7}$$

where $\zeta_n=\pm1$ depending on whether β_n corresponds to positive or negative gain states, and $|\beta_n|\gg1$ is used.

We next evaluate Eq. (B6) for the case of one positive gain loosely bound mode, i.e., $|\mathrm{Im}\beta_n|\ll|\mathrm{Re}\beta_n|$. After a straightfoward Taylor expansion of the bound-mode resonant denominators in Eq. (B7), we finally obtain

$$I_{b\text{-}b}^{(n)}=I_{f\text{-}f}^{(n)}=-I_{b\text{-}f}^{(n)}=-I_{f\text{-}b}^{(n)}\ , \tag{B8}$$

so that

$$I_{\mathrm{tot}}^{(n)}=0\ . \tag{B9}$$

[1] B. J. MacGowan *et al.*, Phys. Rev. Lett. **65**, 420 (1990).
[2] R. A. London, M. D. Rosen, and J. E. Trebes, Appl. Opt. **28**, 3397 (1989).
[3] D. L. Matthews (private communication).
[4] J. E. Trebes (private communication).
[5] R. A. London, M. D. Rosen, and M. Strauss, Phys. Rev. Lett. **65**, 563 (1990).
[6] M. D. Rosen, J. E. Trebes, and D. L. Matthews, Comments Plasma Phys. Controlled Fusion **10**, 245 (1987).
[7] C. H. Henry, J. Lightwave Tech. LT-**4**, 288 (1986).
[8] G. Hazak and A. Bar-Shalom, Phys. Rev. A **38**, 1300 (1988); **40**, 7055 (1989).
[9] H. A. Haus and S. Kawakami IEEE J. Quantum Electron. **QE-21**, 63 (1985).
[10] A. E. Siegman, Phys. Rev. A **39**, 1253 (1989); **39**, 1264 (1989).
[11] J.-L. Doumont, P. L. Mussche, and A. E. Siegman, IEEE J. Quantum Electron. **QE-25**, 1960 (1989); P. L. Mussche

and A. E. Siegman, in *Laser Noise,* edited by R. Roy (SPIE, Boston, 1990), pp. 153–163; P. W. Milonni, *ibid.*, pp. 164–171; I. H. Deutsch, J. C. Garrison, and E. M. Wright, J. Opt. Soc. Am. B **8**, 1244 (1991).

[12] K. Petermann, IEEE J. Quantum Electron. **QE-15**, 566 (1979).

[13] M. Strauss, Phys. Fluids B **1**, 907 (1989).

[14] N. G. Basov, V. N. Morozov, and A. N. Oraevskii, Zh. Eksp. Teor. Fiz. **49**, 895 (1965) [Sov. Phys.—JETP **22**, 622 (1966)]; A. F. Suchkov, *ibid.* **49**, 1495 (1965) [*ibid.* **22**, 1026 (1966)]; R. G. Allakhverdyan, A. N. Oraevskii, and A. F. Suchkov, Fiz. Tekh. Poluprovodn. **4**, 341 (1970) [Sov. Phys. Semicond. **4**, 277 (1970)]; V. E. Kuzin and A. F. Suchkov, Kvant. Elektron. (Moscow) **3**, 53 (1972) [Sov. J. Quantum Electron. **2**, 236 (1972)]; J. Buus, IEEE J. Quantum Electron. **QE-19**, 953 (1983); P. K. Cheo, *Fiber Optics, Devices and Systems* (Prentice-Hall, Englewood, Cliffs, NJ, 1985), pp. 180–191; L. A. Lugiato, C. Oldano, and L. M. Narducci, J. Opt. Soc. Am. B **5**, 879 (1988); R. Lefever, L. A. Lugiato, W. Kaige, N. B. Abraham, and P. Mandel, Phys. Lett. A **135**, 254 (1989).

[15] A. E. Siegman, *Lasers* (University Science, Mill Valley, CA 1986).

[16] G. Arfken, *Mathematical Methods for Physicists,* 2nd ed. (Academic, New York, 1970).

[17] M. Born and E. Wolf, *Principles of Optics,* 4th ed. (Pergamon, New York, 1970).

[18] J. W. Goodman, *Statistical Optics* (Wiley-Interscience, New York, 1985).

[19] R. E. Collins, *Field Theory of Guided Waves* (McGraw-Hill, New York, 1960); W. W. Anderson, IEEE J. Quantum Electron. **QE-1**, 228 (1965); S. J. Chua and B. Thomas, Opt. Quantum Electron. **9**, 15 (1977); W. Streifer, D. R. Scrifes, and R. D. Burkham, IEEE J. Quantum Electron. **QE-14**, 418 (1978); K. Petermann, Opt. Quantum Electron. **13**, 323 (1981); T. Kambayashi and J. Sarma, IEEE J. Quantum Electron. **QE-19**, 1084 (1983).

[20] The minus branch of the complex square root of E_n is chosen here in order to guarantee physically plausible laserlike modes that grow in z and decay in x away from the lasing medium. Thus, we adopt the convention throughout that $\mathrm{Re}(\beta)<0$ and $\mathrm{Im}(\beta)>0$ for all eigenmodes of Eq. (4).

[21] M. D. Rosen *et al.,* Phys. Rev. Lett. **54**, 106 (1985); D. L. Matthews *et al., ibid.* **54**, 110 (1985).

[22] Actually, these spurious modes reemerge mathematially as first-order poles or resonances for a contour integral of intensity in the spontaneous-emission stage (see Appendix B).

[23] G. Baym, *Lectures on Quantum Mechanics* (Benjamin, Reading, MA, 1977).

[24] L. D. Landau and E. M. Lifshitz, *Quantum Mechanics* (Pergamon, New York, 1976).

[25] We must be careful to include only those bound modes which also satisfy the criterion: $k_\perp/k \leq A/L$ in the case of Eq. (30) or $k_\perp/k \leq 2a/L$ when Eq. (31) is used.

[26] M. Feit and J. Fleck, J. Opt. Soc. Am. B 7, 2048 (1990).

[27] S. J. Kuo, D. T. Smithey, and M. G. Raymer, Phys. Rev. Lett. **66**, 2605 (1991).

[28] We understand α_n to actually mean α_E for the free modes under discussion here.

[29] We note that in extending β and β' into the complex plane, all values are allowed including the eigenvalues of Eq. (4).